JOC The Journal of Organic Chemistry

pubs.acs.org/joc Article

Self-Assembled 2,3-Dicyanopyrazino Phenanthrene Aggregates as a Visible-Light Photocatalyst

Min He, Xiaoqiang Yu,* Yi Wang, Fei Li, and Ming Bao*

Cite This: J. Org. Chem. 2021, 86, 5016−5025 Read Online

ACCESS | Metrics & More | Article Recommendations | Supporting Information

ABSTRACT: In this study, 2,3-dicyanopyrazino phenanthrene (**DCPP**), a commodity chemical that can be prepared at an industrial scale, was used as a photocatalyst in lieu of Ru or Ir complexes in C−X (X = C, N, and O) bond-forming reactions under visible-light irradiation. In these reactions, $[\mathbf{DCPP}]_n$ aggregates were formed *in situ* through physical $\pi-\pi$ stacking of **DCPP** monomers in organic solvents. These aggregates exhibited excellent photo- and electrochemical properties, including a visible light response (430 nm), long excited-state lifetime (19.3 μs), high excited-state reduction potential ($E_{red}([\mathbf{DCPP}]_n^*/[\mathbf{DCPP}]_n^{\cdot-})$ = +2.10 V vs SCE), and good reduction stability. The applications of $[\mathbf{DCPP}]_n$ aggregates as a versatile visible-light photocatalyst were demonstrated in decarboxylative C−C cross-coupling, amidation, and esterification reactions.

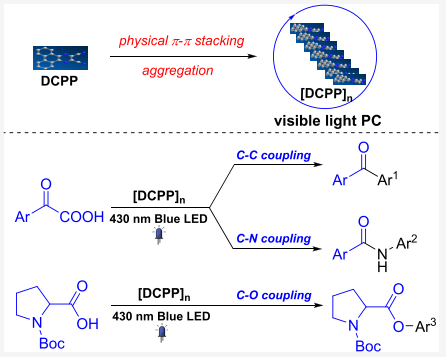

INTRODUCTION

Visible-light photocatalytic reactions have attracted increasing attention in recent years because of their mild conditions, green economy, and easier control than heat-driven reactions.[1] Photocatalysts that activate organic substrates through electron transfer[2] or energy transfer[3] have thus gained rapid development. As a typical visible-light photocatalyst class, organometallic complexes, such as those involving Ru and Ir metals,[4] usually suffer from being expensive, potentially toxic, and poorly sustainable.[5] In contrast, in recent years, organic dyes, including xanthene,[6] acridinium salts,[7] and 4CzIPN,[8] have shown excellent potential as photocatalysts in visible-light-driven reactions because of their low toxicity and easily modifiable chemical structures (Scheme 1, previous work). These organic dyes usually contain a D−π−A molecular structure and require complicated and tedious synthetic routes that generate large amounts of waste and incur high costs. These characteristics hinder their large-scale application. Simple aromatic derivatives that are abundant and readily available are considered to be ideal photocatalysts in the industry. However, most of these compounds only absorb light in the ultraviolet region. Whether these simple aromatic derivatives can be used directly as photocatalysts in visible-light-induced reactions remains a point of interest.

In recent years, aggregation has been proven to be a useful tool in bio-organic chemistry and physical organic chemistry.[9] Aggregates can be built through the $\pi-\pi$ stacking of small molecules and exhibit distinctive chemical, optical, and electrical properties.[10] For example, the aggregation of benzene and naphthalene systems at high concentrations in organic solvents can present a low-energy absorption band.[11] This change is important for visible-light-induced reactions wherein

Scheme 1. Visible-Light Photocatalysts in Organic Transformation Reactions

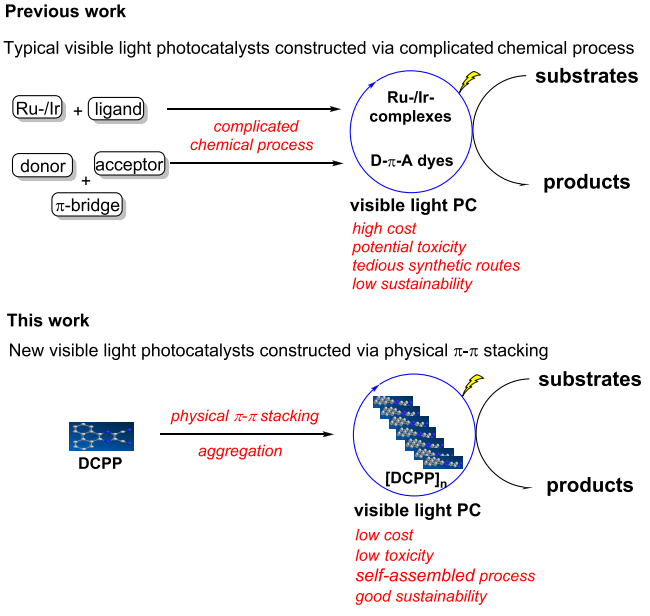

Received: December 14, 2020
Published: March 15, 2021

https://dx.doi.org/10.1021/acs.joc.0c02945
J. Org. Chem. 2021, 86, 5016−5025

aromatic derivative aggregates are used as photocatalysts. Strategies based on the fact that aggregates absorb visible light by association of an electron-rich substrate with an electron-accepting molecule, called an electron donor−acceptor (EDA) complex, have been developed.[12] Our present work is inspired by the reports of Tang and co-workers who found that aromatic rings bearing neighboring fluorophores can promote the formation of aggregates through strong $\pi-\pi$ stacking interactions.[13] We wondered whether the aromatic rings bearing neighboring fluorophores, including 1,4-dicyanobenzene (**DCB**), 1,4-naphthoquinone (**1,4-NQ**), fluorenone (**FLN**), anthrone (**ANN**), anthraquinone (**AQ**), 9,10-phenanthraquinone (**PQ**), and 2,3-dicyanopyrazino phenanthrene (**DCPP**)[14] (Figure 1), could aggregate through $\pi-\pi$ stacking

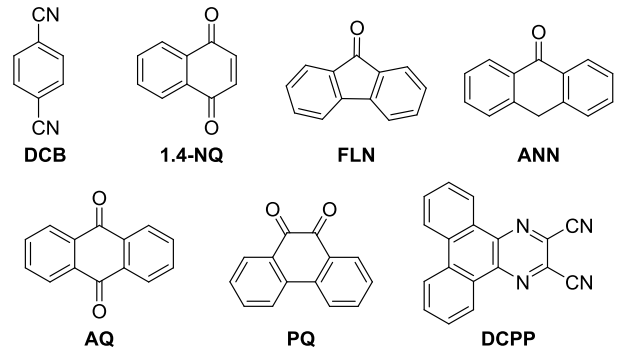

Figure 1. Simple aromatic derivatives.

in organic solvents to extend their absorption to the visible-light region and whether their aggregates formed *in situ* in organic solvents could be used as photocatalysts in visible-light-induced organic reactions (Scheme 1, this work).

RESULTS AND DISCUSSION

We began our investigations by acquiring UV−vis absorption spectra. As shown in Figure 2a, all seven aromatic derivatives had almost no absorption in the visible-light region at a concentration of 10^{-5} M. When the concentration of the derivatives was increased to 10^{-3} M, compounds **FLN**, **ANN**, **AQ**, **PQ**, and **DCPP** showed absorption in the 400−500 nm region (Figure 2b). Notably, the normalized absorbance spectra of **DCPP** did not match well with each other at different concentrations. This discrepancy indicated that the prominent visible-light region absorbance was caused not only by concentration but also by specific interactions between **DCPP** molecules (Figure 2d). We ascribed the red shift to the *in situ* formation of aggregates through physical $\pi-\pi$ stacking at high concentrations in *N*,*N*-dimethylformamide (DMF). In particular, the electron-accepting CN on the **DCPP** aromatic ring could deplete the density of aryl π electrons through π-resonance effects, thus reducing electron−electron repulsion between the π electron clouds of the stacking rings and enhancing π-stacking interactions.

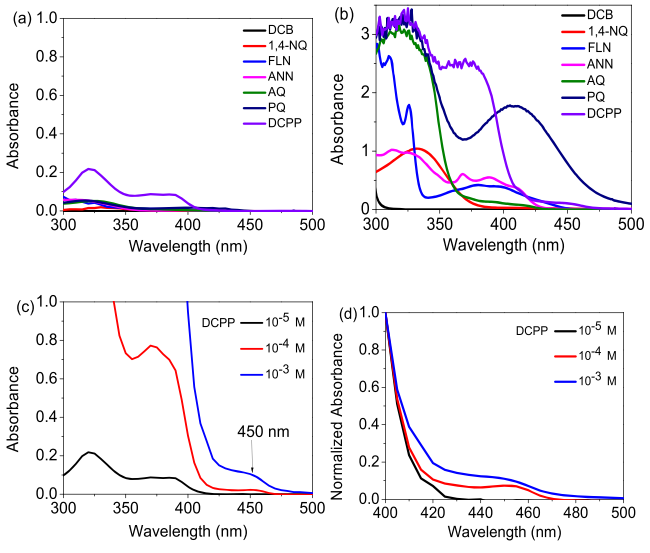

Figure 2. UV−vis absorption spectra of all the compounds at different concentrations in DMF: (a) $c = 10^{-5}$ M and (b) $c = 10^{-3}$ M. (c) Absorption spectra and (d) normalized absorption spectra of **DCPP** at different concentrations (10^{-5}−10^{-3} M) in DMF.

Next, the emission spectra of **DCPP** at different concentrations in DMF were examined (Figure 3) to further prove the *in situ* formation of $[\mathbf{DCPP}]_n$ aggregates. The emission wavelength showed a blue shift from 512 to 473 nm as the excitation wavelength increases from 380 to 450 nm (Figure 3a). A wavelength shift from 490 nm (10^{-5} M) to 508 nm (10^{-3} M) was observed at a 430 nm excitation wavelength (Figure 3b); these shifts indicated a change in emission, probably caused by aggregates through $\pi-\pi$ stacking.[15] In addition, the emission intensity at 514 nm ($\lambda_{excitation}$ = 380 nm) is not proportional to the concentration of **DCPP**, indicating that the emission does not originate from monomeric **DCPP** species (Figure 3c,d).[16]

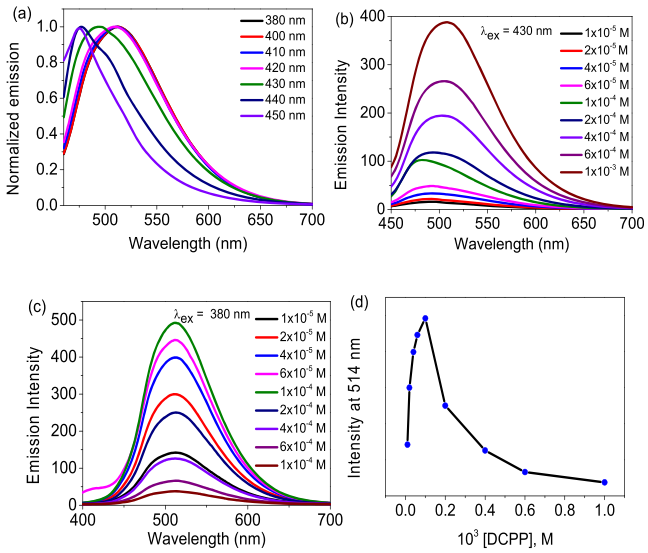

Figure 3. (a) Normalized emission spectra of **DCPP** ($c = 1 \times 10^{-4}$ M) at different excitation wavelengths in DMF. Emission spectra of **DCPP** at different concentrations (from 1×10^{-5} M to 1×10^{-3} M in DMF): (b) $\lambda_{excitation}$ = 430 nm and (c) $\lambda_{excitation}$ = 380 nm. (d) Concentration dependence of emission spectra at 514 nm ($\lambda_{excitation}$ = 380 nm).

As shown in Figure 4a, the particle size of $[\mathbf{DCPP}]_n$ aggregates in DMF with different concentrations was characterized through dynamic light scattering (DLS). We found that the particle size of $[\mathbf{DCPP}]_n$ increased with the increase in concentration and the effective diameters are 558 nm at a concentration of 10^{-4} M and 1059 nm at a concentration of 10^{-3} M. Transmission electron microscopy

https://dx.doi.org/10.1021/acs.joc.0c02945
J. Org. Chem. 2021, 86, 5016−5025

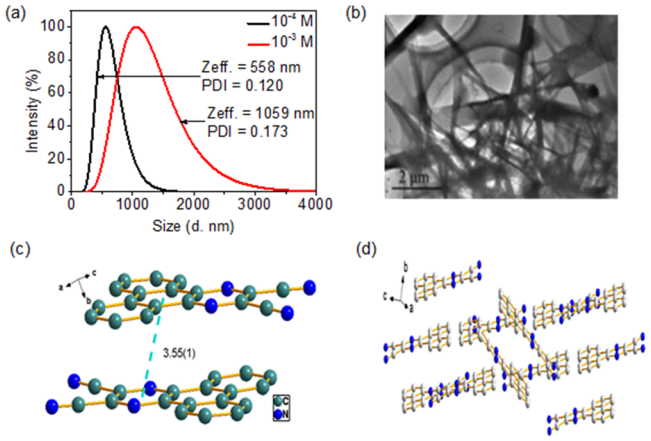

Figure 4. (a) DLS of **DCPP** at different concentrations in DMF (10^{-4} and 10^{-3} M). (b) TEM images of **DCPP** in DMF and amount of water (1.0×10^{-4} M). (c) Measured distance between two molecules of **DCPP** in the crystal structure. (d) Packing diagram of **DCPP**.

(TEM) provided direct evidence for the presence of extended $\pi-\pi$ stacking networks, as shown in Figure 4b. Single-crystal X-ray diffraction analysis has shown that adjacent molecules are in close proximity, allowing $\pi-\pi$ stacking interactions between a benzene ring and pyrazine ring. The crystallographically independent **DCPP** molecules are almost parallel to each other, with molecules arranged in an antiparallel fashion at a centroid−centroid distance of 3.55 Å (Figure 4c,d).

Encouraged by this initial outcome, we studied the visible-light-induced decarboxylative coupling of α-oxocarboxylic acids with aryl iodides to investigate the feasibility of using these simple aromatic derivatives as photocatalysts in lieu of typical visible-light photocatalysts, such as $(Ir[dF\{CF_3\}ppy]_2[dtbbpy])PF_6$.[17] We began our investigation with the decarboxylative cross-coupling of phenylglyoxylic acid (**1a**) with *p*-iodotoluene (**2a**) as a model reaction in the presence of photo/palladium dual catalysts to confirm whether or not such a reaction would occur. Thus, we added the photocatalyst (2.5 mol %, equal to a 10^{-3} M concentration) and $Pd(dba)_2$ (3 mol %) to a solution of **1a** (0.4 mmol), **2a** (0.2 mmol), and K_2HPO_4 (0.4 mmol) in DMF (5.0 mL) under a nitrogen atmosphere. The mixture was stirred at room temperature under irradiation with a 10 W blue LED. The preliminary results are summarized in Table 1. The use of benzene and naphthalene derivatives (**DCB** and **1,4-NQ**) as photocatalysts was initially examined, but no reaction was observed (entries 1 and 2). However, to our delight, the desired product **3a** was obtained in 53% yield by using **FLN** as a photocatalyst (entry 3). The activities of anthracene and phenanthrene derivatives (**ANN**, **AQ**, **PQ**, and **DCPP**) as photocatalysts in the present method (entries 4−7) were examined next. **DCPP** exhibited the best photocatalytic activity, providing **3a** in 77% yield (entry 7). LED wavelengths were subsequently screened by using **DCPP** as a photocatalyst. Among the tested wavelengths (365, 400, 430, and 450 nm), the 430 nm LED provided the highest yield (entries 7−10). No reaction was observed in the absence of light radiation (entry 11). When the **DCPP** loading was increased to 5 mol %, the yield of **3a** increased to 91% (entry 12). However, when the catalyst loading was decreased to 0.5 mol % (equal to a 2×10^{-4} M concentration), **3a** was obtained in only 19% (entry 13). When further reducing the amount of catalyst to 0.05 mol % (equal to a 2×10^{-5} M concentration), **3a** was not detected at all (entry 14). Substrate concentration was next examined. It was found that the reaction yield with 1 mol % (entry 15) and 2.5 mol % (entry 16) **DCPP** loadings at 0.4 and 0.16 M of **1a**, respectively, gave low to moderate yields compared to a 5 mol % **DCPP** loading. These results suggest that the real photocatalyst is the aggregates $[\mathbf{DCPP}]_n$ rather than single-molecule **DCPP**. When this reaction was performed under an air atmosphere, **3a** was produced in only 53% yield (entry 17). Therefore, the subsequent decarboxylative reactions of acid substrate **1** with aryl iodide **2** were performed by using conditions specified in entry 12.

Table 1. Screening of the Decarboxylative Cross-Coupling of Phenylglyoxylic Acid with *p*-Iodotoluene[a]

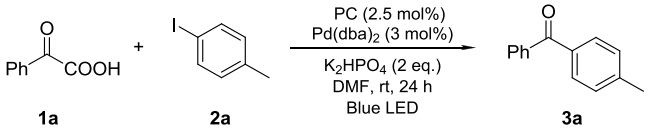

1a **2a** **3a**

entry	photocat.	light source	yield (%)[b]
1	**DCB**	10 W 430 nm blue LED	0
2	**1,4-NQ**	10 W 430 nm blue LED	0
3	**FLN**	10 W 430 nm blue LED	53
4	**ANN**	10 W 430 nm blue LED	0
5	**AQ**	10 W 430 nm blue LED	50
6	**PQ**	10 W 430 nm blue LED	5
7	**DCPP**	10 W 430 nm blue LED	77
8	**DCPP**	10 W 365 nm blue LED	37
9	**DCPP**	10 W 400 nm blue LED	52
10	**DCPP**	10 W 450 nm blue LED	61
11	**DCPP**	no light	0
12[c]	**DCPP**	10 W 430 nm blue LED	91
13[d]	**DCPP**	10 W 430 nm blue LED	19
14[e]	**DCPP**	10 W 430 nm blue LED	0
15[f]	**DCPP**	10 W 430 nm blue LED	25
16[g]	**DCPP**	10 W 430 nm blue LED	66
17[h]	**DCPP**	10 W 430 nm blue LED	53

[a]Reaction conditions: **1a** (0.4 mmol) and **2a** (0.2 mmol), **PC** (2.5 mol %), $Pd(dba)_2$ (3 mol %), K_2HPO_4 (0.4 mmol), DMF (5 mL), irradiation with a 10 W 430 nm blue LED, rt, 24 h. [b]Isolated yield. [c]**DCPP** catalyst (5 mol %) was used. [d]**DCPP** catalyst (0.5 mol %) was used. [e]**DCPP** catalyst (0.05 mol %) was used. [f]**1a** (2 mmol) and **2a** (1 mmol), $Pd(dba)_2$ (15 mol %), K_2HPO_4 (2 mmol). [g]**1a** (0.8 mmol) and **2a** (0.4 mmol), $Pd(dba)_2$ (6 mol %), K_2HPO_4 (0.8 mmol). [h]Reaction was performed under air.

Following identification of the optimal reaction conditions, reactions of aryl iodides **2a−2s** with **1a** were conducted to examine the substrate generality. The results are summarized in Scheme 2. In addition to **2a**, aryl iodides **2b−2f** with methyl and methoxyl on the phenyl ring provided the corresponding products **3b−3f** in good to high yields. Notably, owing to the steric hindrance effect, the *ortho*-substituted substrates **2b** and **2e** gave lower yields than those with *para*- and *meta*-substituents (**2a**, **2c**, **2d**, and **2f**). The reactions of substrates **2i−2n**, which bear electron-withdrawing groups (COMe, CHO, CO_2Et, CN, and CF_3) on their benzene rings, afforded the corresponding desired products **3i−3n** in high yields. These results indicated that the electronic property of the substituent on the benzene ring did not influence the reactivity of the iodide substrates. This transformation also tolerated aryl iodides with the halogen functional groups fluoro (**2o**), chloro (**2p**), and bromo (**2q**) to afford products **3o−3q** in satisfactory

https://dx.doi.org/10.1021/acs.joc.0c02945
J. Org. Chem. 2021, 86, 5016−5025

Scheme 2. Scope Evaluation of Aryl Iodides[a]

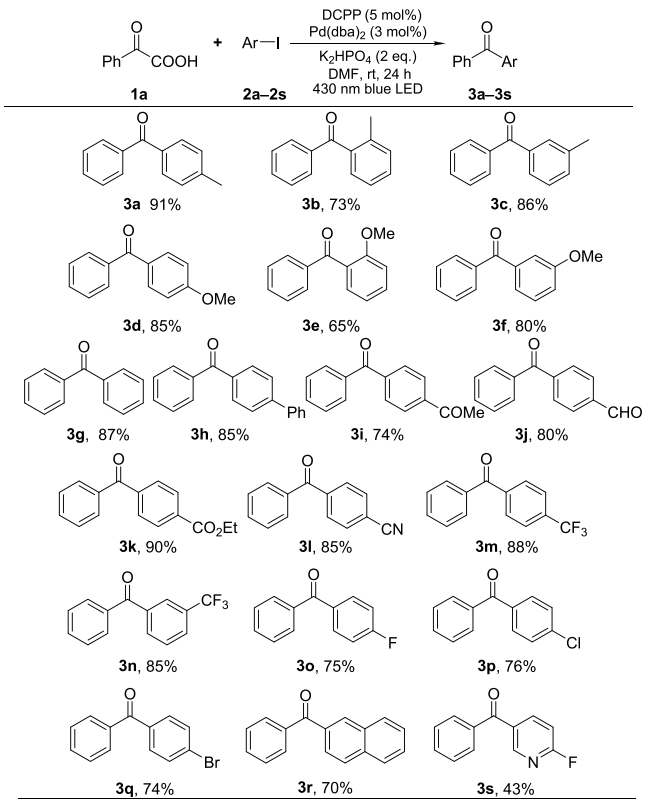

[a]Reaction conditions: **1a** (0.4 mmol) and **2a**–**2s** (0.2 mmol), **DCPP** (5 mol %), $Pd(dba)_2$ (3 mol %), K_2HPO_4 (0.4 mmol), DMF (5 mL), irradiation with a 10 W 430 nm blue LED, rt, 24 h.

yields. Iodonaphthalene **2r** was also suitable for use in the present method to produce **3r** in 70% yield. Notably, the heterocyclic substrate 2-fluoro-5-iodopyridine (**2s**) also worked, albeit with relatively lowered reactivity.

Next, the evaluation of the scope of α-oxocarboxylic acids under the optimized conditions was conducted and the result is summarized in Scheme 3. The reactions of arylglyoxylic acids **1b** and **1c**, which possess electron-donating groups (MeO and Me) on their benzene rings, afforded the corresponding products with good yields. However, a low **3d′** yield (10%) was observed when **2a** was treated with **1d**, which bears a CF_3 group on its benzene ring. These results indicated that the reactivity of the arylglyoxylic acid substrate was remarkably influenced by the electronic properties of the aromatic ring. Of note, the aliphatic keto acids **1h**−**1j** were also suitable for use in the reaction to afford the corresponding ketones **3h′**−**3j′** in good yields (86%−88%).

Scheme 3. Scope Evaluation of α-Oxocarboxylic Acids[a]

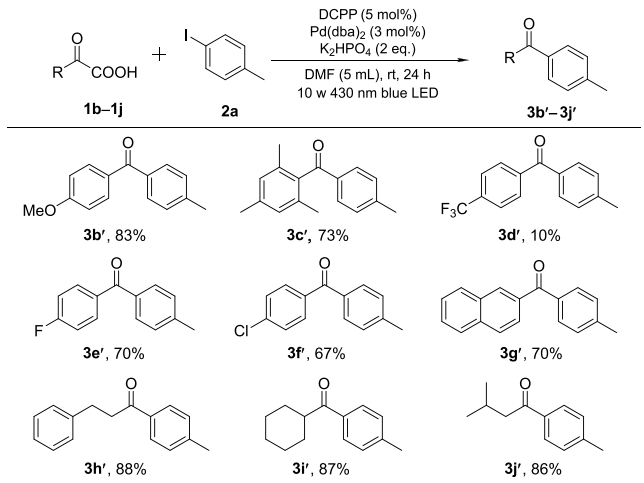

[a]Reaction conditions: **1b**−**1j** (0.4 mmol) and **2a** (0.2 mmol), **DCPP** (5 mol %), $Pd(dba)_2$ (3 mol %), K_2HPO_4 (0.4 mmol), DMF (5 mL), irradiation with a 10 W 430 nm blue LED, rt, 24 h.

A plausible catalytic cycle was proposed and is shown in Scheme 4. Initially, $[\mathbf{DCPP}]_n$ aggregates could be formed *in situ* in solvents through the $\pi-\pi$ stacking of ***n*DCPP**, and its absorption region was extended to 500 nm (Figure 2c). Under visible-light irradiation, $[\mathbf{DCPP}]_n$ was excited to generate $[\mathbf{DCPP}]_n$*. The base-mediated deprotonation of phenylglyoxylic acid and the subsequent single-electron oxidation of the resulting carboxylate functionality by $[\mathbf{DCPP}]_n$* in its excited state generated the corresponding acyl radical species **I** (upon CO_2 extrusion), which was trapped by 2,2,6,6-tetramethyl-1-piperidinyloxyl to its adduct **II** in 80% isolated yield along with the formation of $[\mathbf{DCPP}]_n^{\cdot-}$. Meanwhile, the second catalytic cycle was initiated by the oxidative addition of the Pd^0 catalyst with PhI to generate Pd^{II} complex **III**. The acyl radical was then rapidly captured by Pd^{II} complex **III** to generate Pd^{III} complex **IV**, which was subsequently reduced by $[\mathbf{DCPP}]_n^{\cdot-}$ to form Pd^{II} complex **V**. Finally, Pd^{II} complex **V** underwent reductive elimination to afford the product and close the palladium catalytic cycle.

Scheme 4. Proposed Mechanism of $[\mathbf{DCPP}]_n$/Pd-Catalyzed Decarboxylative Coupling

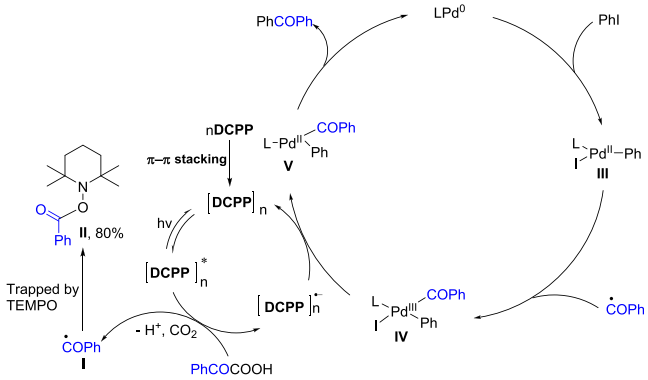

Next, the photoelectronic kinetics of $[\mathbf{DCPP}]_n$ was studied by transient absorption spectroscopy.[18] As shown in Figure 5a, the decay at 420 nm corresponds to the long-lived excited state of $[\mathbf{DCPP}]_n$* ($\tau = 37.09\%\tau_1 + 62.91\%\tau_2 = 19.3\ \mu s$), which was active for reductive quenching by α-oxocarboxylic acids. The cyclic voltammogram shown in Figure 5b indicated a high excited-state reduction potential ($E_{red}([\mathbf{DCPP}]_n^{*}/[\mathbf{DCPP}]_n^{\cdot-})$ = +2.10 V vs SCE),[19] which was sufficient for oxidizing phenylglyoxylic acid ($E_{1/2}^{ox} \approx +1.0$ V vs SCE) into acyl radical **I** (as proposed in Scheme 4).

The application scope of $[\mathbf{DCPP}]_n$ should therefore be larger than that of $(Ir[dF\{CF_3\}ppy]_2[dtbbpy])PF_6$ ($E_{1/2}^{red}[*Ir^{III}/Ir^{II}]$ = +1.21 V vs SCE).[18] Photocurrent tests were carried out with a 0.1 V bias under visible light (>400 nm) in Figure 5c. $[\mathbf{DCPP}]_n$ (10^{-3} M in DMF) exhibited considerably higher photocurrent response than lower

https://dx.doi.org/10.1021/acs.joc.0c02945
J. Org. Chem. 2021, 86, 5016−5025

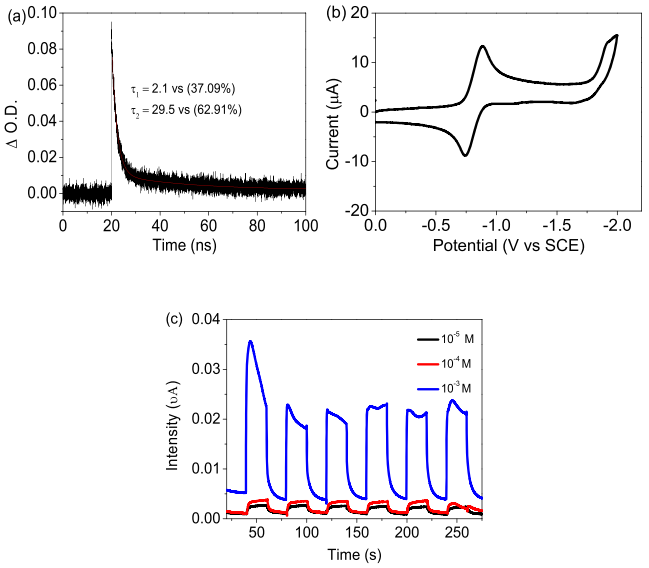

Figure 5. (a) Luminescence decays of **DCPP** at 420 nm. (b) Cyclic voltammetry of **DCPP** (DMF, scan rate: 50 mV s^{-1}). (c) Concentration-dependent photoelectronic responses of **DCPP** in DMF under visible-light irradiation at a bias of 0.1 V.

concentrations (10^{-5} and 10^{-4} M in DMF), suggesting the great separation and transport capability of photocarriers as a result of the enlargement of $[\mathbf{DCPP}]_n$. The result shown here also revealed that $[\mathbf{DCPP}]_n^{\cdot-}$ had high stability, which fulfilled the requirement for the reduction of Pd^{III} complex **IV** into Pd^{II} complex **V**, as proposed in Scheme 4.

Encouraged by the preliminary results of the photoredox reaction, a gram-scale reaction was performed and gave the desired product **3a** in 70% yield (Scheme 5, eq 1). $[\mathbf{DCPP}]_n$

Scheme 5. Applications of $[\mathbf{DCPP}]_n$ in Gram-Scale C−O and C−N Bond-Forming Reactions

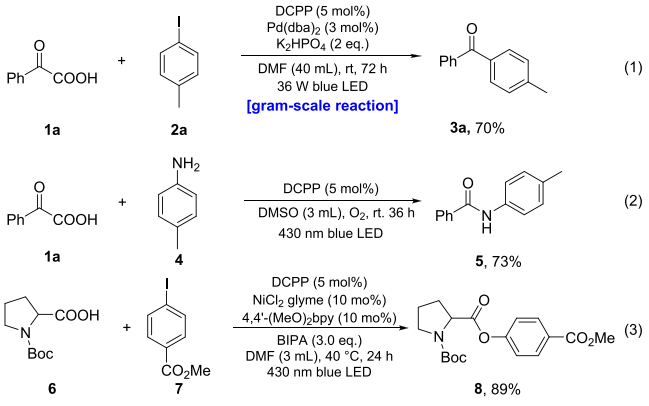

was then applied to visible-light-induced C−O and C−N bond-forming reactions. As demonstrated in Scheme 5 in eq 2, $[\mathbf{DCPP}]_n$ as the photocatalyst in place of a Ru complex[20] in the amidation of **1a** with aniline **4** under visible-light irradiation afforded amide **5** in 73% yield. Moreover, the application of $[\mathbf{DCPP}]_n$ in the esterification of carboxylic acid **6** with aryl iodide **7** was studied by using $NiCl_2$·glyme (glyme = dimethoxyethane), 4,4′-di-OMe-2,2′-dipyridyl (4,4′-$[MeO]_2$bpy), and *N*-*tert*-butylisopropylamine (BIPA). Again, $[\mathbf{DCPP}]_n$ showed similar catalytic activity to the Ir catalyst, affording the C−O coupling product **8** in 89% yield (Scheme 5, eq 3).[21]

CONCLUSIONS

We discovered a new type of $[\mathbf{DCPP}]_n$ aggregate photoredox catalyst that was built through the $\pi-\pi$ stacking of single-molecule **DCPP**. The catalytic activity of $[\mathbf{DCPP}]_n$ aggregates was similar to those of Ir and Ru catalysts in some visible-light-promoted C−X (X = C, N, and O) bond-forming reactions, including the decarboxylation of α-oxocarboxylates with aryl iodides, the amidation of phenylglyoxylic acid with aniline, and the esterification of phenylglyoxylic acid with aryl iodide. Notably, **DCPP** is commercially available and can be prepared at the industrial scale. In contrast to the availability of normal photoredox catalysts, such as Ru complexes, Ir complexes, and D−π−A dyes, the *in situ* formation of aggregates $[\mathbf{DCPP}]_n$ in a certain concentration of organic solvent through physical $\pi-\pi$ stacking confers them great potential as a new type of photocatalyst in organic synthesis. Further investigations on $[\mathbf{DCPP}]_n$ aggregates in visible-light photocatalytic reactions are ongoing.

EXPERIMENTAL SECTION

Materials and Methods. Unless otherwise noted, materials were purchased from commercial suppliers and used without further purification. Solvents were purified by standard techniques without special instructions. Thin-layer chromatography (TLC) was carried out on SiO_2 (silica gel 60 F_{254}, Merck), and the spots were located with UV light. Products were purified by flash chromatography on 200−300 mesh silica gel SiO_2. The ^1H, ^{13}C, and ^{19}F NMR spectra were recorded on a Bruker Avance II-400 spectrometer (400 MHz for ^1H and 100 MHz for ^{13}C); $CDCl_3$ (or DMSO-d_6) and tetramethylsilane (TMS) were used as a solvent and an internal standard, respectively. The chemical shifts are reported in ppm downfield (δ) from TMS; the coupling constants J are given in Hz. The peak patterns are indicated as follows: s, singlet; d, doublet; t, triplet; q, quartet; m, multiplet; and bs, broad singlet. UV−vis spectra were obtained on a Lambda 750S and Agilent 8453 UV−vis spectrophotometer. A JASCO FP-6500 spectrophotometer was used to acquire the fluorescence spectra. The morphologies and sizes of the aggregate photocatalyst were examined through a JEM-2000 transmission electron microscope (TEM) and Brookhaven-Omni dynamic light scattering (DLS) instrument. X-ray intensity data were measured on a Bruker SMART APEX CCD. Transient absorption spectrum and luminescence decay were obtained using an LP920 (Edinburgh Instruments Ltd.) Nd:YAG laser spectrometer. Electrochemical potential was obtained with a standard set of conditions to maintain internal consistency on a BAS 100 W electrochemical analyzer. Samples for electrochemical measurements were prepared with 10 mL of a 0.1 M tetrabutylammonium hexafluorophosphate (NBu_4PF_6) solution in DMF and 0.01 mmol of substrate. Measurements employed a radium glassy carbon working electrode, platinum wire counter electrode, and saturated calomel electrode (SCE). The scan rate for the CV measurements was 50 mV/s. Photoelectronic responses were carried out on a Keithley 2450 (USA).

Synthesis of 2,3-Dicyanopyrazino Phenanthrene.[14] A mixture of 9,10-phenanthrenequinone (1.00 g), diaminodicyanoethane (0.54 g), ethanol (60 mL), and acetic acid (1 mL) was refluxed with stirring for 12 h in an oil bath. After cooling to room temperature, the resulting solid product was collected and recrystallized from DMF to give compound **DCPP** in 83% yield (1.12 g).

Synthesis of α-Oxocarboxylic Acids. The α-oxocarboxylic acids (**1b**, **1d**, **1e**, and **1g**) were prepared from oxidation of corresponding methyl ketones by SeO_2 according to the reported procedure.[23] A mixture of aryl-methylketone (1 mmol) and selenium dioxide (0.33 g, 3 mmol) in dry pyridine (20 mL) was stirred at 110 °C under nitrogen for 1 h in an oil bath, and then the bath temperature was

https://dx.doi.org/10.1021/acs.joc.0c02945
J. Org. Chem. 2021, 86, 5016−5025

reduced to 90 °C. The mixture was stirred at 90 °C, and progress of the reaction was monitored by TLC. The desired products were isolated by silica-gel column chromatography (ethyl acetate:petroleum ether = 1:10).

Representative Procedure for the Decarboxylation of α-Oxocarboxylates with Aryl Iodides. To a dried 20 mL reaction tube were charged α-oxocarboxylic acid (**1a**, 60 mg, 0.4 mmol), *p*-methyl iodobenzene (**2a**, 44 mg, 0.2 mmol), K_2HPO_4 (70 mg, 0.4 mmol), **DCPP** (2.8 mg, 5 mol %), and $Pd(dba)_2$ (3.5 mg, 3 mol %). The tube was capped. After being evacuated and backfilled with nitrogen three times, DMF (5 mL) was added via a gastight syringe. The reaction mixture was stirred at room temperature under the irradiation of a 10 W 430 nm blue LED for 24 h. The mixture was quenched with water and extracted with ethyl acetate (3 × 10 mL), and the combined organic layers were dried over Na_2SO_4. The solvent was removed under reduced pressure, and the residue obtained was purified via silica gel chromatography (ethyl acetate:petroleum ether = 1:50) to afford phenyl(*p*-tolyl)methanone (**3a**, 36.2 mg, 91% yield).

Decarboxylation of α-Oxocarboxylic Acid with *p*-Methylaniline. To a dried 20 mL reaction tube were charged α-oxocarboxylic acid (**1a**, 75 mg, 0.5 mmol), *p*-methylaniline (**4**, 70 mg, 0.75 mmol), and **DCPP** (7 mg, 5 mol %). The tube was capped. After being evacuated and backfilled with O_2 three times, DMSO (3 mL) was added via a gastight syringe. The reaction mixture was stirred under the irradiation of a 10 W 430 nm blue LED at room temperature for 36 h. After 36 h, the mixture was quenched with water and extracted with ethyl acetate (3 × 10 mL). The combined organic layers were dried over Na_2SO_4 and concentrated under vacuo. The product was purified by flash column chromatography on a silica gel (ethyl acetate:petroleum ether = 1:10) to afford *N*-phenylbenzamide (**5**, 77.5 mg, 73% yield).

Esterification of 1-(*tert*-Butoxycarbonyl)-L-proline with 4-Iodobenzoate. To a dried 20 mL reaction tube were charged nickel(II) chlorine·diglyme (4.4 mg, 10 mol %), 4,4′-di-methoxy-2,2′-dipyridyl (4.3 mg, 10 mol %), **DCPP** (2.8 mg, 5 mol %), 1-(*tert*-butoxycarbonyl)-L-proline (**6**, 65 mg, 0.3 mmol), and methyl 4-iodobenzoate (**7**, 52 mg, 0.2 mmol). The tube was capped. After being evacuated and backfilled with nitrogen three times, DMF (3 mL) was added via a gastight syringe followed by the addition of *N*-*tert*-butyl-isopropylamine (95 μL, 0.6 mmol, 3.0 equiv). The reaction mixture was stirred under the irradiation of a 10 W 430 nm blue LED at 40 °C for 24 h. After 24 h, the mixture was quenched with water and extracted with ethyl acetate (3 × 10 mL). The combined organic layers were dried over Na_2SO_4 and concentrated under vacuo. The product was purified by flash column chromatography on a silica gel (ethyl acetate:petroleum ether = 1:5) to afford 1-(*tert*-butyl) 2-(4-(methoxycarbonyl)phenyl)pyrrolidine-1,2-dicarboxylate (**8**, 62.3 mg, 89% yield).

TEMPO Trapping Experiments. To a dried 20 mL reaction tube were charged α-oxocarboxylic acid (**1a**, 60 mg, 0.4 mmol), *p*-methyl iodobenzene (**2a**, 44 mg, 0.2 mmol), K_2HPO_4 (70 mg, 0.4 mmol), **DCPP** (2.8 mg, 5 mol %), $Pd(dba)_2$ (3.5 mg, 3 mol %), and TEMPO (93.8 mg, 0.6 mmol, 3.0 equiv). The tube was capped. After being evacuated and backfilled with nitrogen three times, DMF (5 mL) was added via a gastight syringe. The reaction mixture was stirred at room temperature under the irradiation of a 10 W 430 nm blue LED for 24 h. The mixture was quenched with water and extracted with ether acetate (3 × 10 mL), and the combined organic layers were dried over Na_2SO_4. The solvent was removed under reduced pressure, and the residue obtained was purified via silica gel chromatography (ethyl acetate:petroleum ether = 1:50) to afford a TEMPO adduct (**3a″**, 42.3 mg, 80% yield).

Gram-Scale Procedure. To a dried 100 mL reactor were charged α-oxocarboxylic acid (**1a**, 2.4 g, 16 mmol), *p*-methyl iodobenzene (**2a**, 1.75 g, 8 mmol), K_2HPO_4 (2.77 g, 16 mmol), **DCPP** (112 mg, 5 mol %), and $Pd(dba)_2$ (140 mg, 3 mol %). After being evacuated and backfilled with nitrogen three times, DMF (40 mL) was added via a gastight syringe. The reaction mixture was stirred at room temperature under the irradiation of a 36 W blue LED for 72 h. The mixture was quenched with water and extracted with ethyl acetate, and the combined organic layers were dried over Na_2SO_4. The solvent was removed under reduced pressure, and the residue obtained was purified via silica gel chromatography (ethyl acetate:petroleum ether = 1:50) to afford the adduct (**3a**, 1.1 g, 70% yield).

Characterization of Products. *2,3-Dicyanopyrazino Phenanthrene (DCPP).*[14] Yellow solid (1.12 g, 83% yield), mp 200−202 °C. ^1H NMR (400 MHz, $CDCl_3$) δ 9.20 (dd, *J* = 8.0 Hz, 1.6 Hz, 2H), 8.66 (d, *J* = 8.4 Hz, 2H), 7.99−7.95 (m, 2H), 7.86−7.82 (m, 2H); $^{13}C\{^1H\}$ NMR (100 MHz, $CDCl_3$) δ 142.8, 133.2, 132.7, 130.1, 128.9, 127.3, 127.1, 123.2, 113.8.

p-Methoxybenzoylformic Acid (1b).[22] Purification by column chromatography on a silica gel (ethyl acetate:petroleum ether = 1:10) afforded **1b** as a white solid (153 mg, 85%). ^1H NMR (400 MHz, DMSO-d_6) δ 7.89−7.86 (m, 2H), 7.04−7.00 (m, 2H), 3.83 (s, 3H).

4-Trifluoromethylbenzoic Acid (1d).[22] Purification by column chromatography on a silica gel (ethyl acetate:petroleum ether = 1:10) afforded **1d** as a white solid (154 mg, 71%). ^1H NMR (400 MHz, DMSO-d_6) δ 8.09 (d, *J* = 7.6 Hz, 2H), 7.87 (d, *J* = 7.6 Hz, 2H).

2-(4-Fluorophenyl)-2-oxoacetic Acid (1e).[22] Purification by column chromatography on a silica gel (ethyl acetate:petroleum ether = 1:10) afforded **1e** as a yellow solid (126 mg, 75%). ^1H NMR (400 MHz, DMSO-d_6) δ 8.04−8.00 (m, 2H), 7.45−7.41 (m, 2H).

2-(Naphthalen-2-yl)-2-oxoacetic Acid (1g).[23] Purification by column chromatography on a silica gel (ethyl acetate:petroleum ether = 1:10) afforded **1g** as a white solid (160 mg, 80%). ^1H NMR (400 MHz, DMSO-d_6) δ 8.47 (s, 1H), 8.07−7.91 (m, 4H), 7.67−7.57 (m, 2H).

Phenyl(p-tolyl)methanone (3a).[23] Purification by column chromatography on a silica gel (ethyl acetate:petroleum ether = 1:50) afforded **3a** as a white solid (35.8 mg, 91% yield), mp 57−58 °C (lit.[24] 56−57 °C); TLC (PE:EA, 10:1 v/v): R_f = 0.65; ^1H NMR (400 MHz, $CDCl_3$) δ 7.79−7.77 (m, 2H), 7.73 (d, *J* = 8.0 Hz, 2H), 7.59−7.55 (m, 1H), 7.49−7.46 (m, 2H), 7.28 (d, *J* = 8.0 Hz, 2H), 2.44 (s, 3H); $^{13}C\{^1H\}$ NMR (100 MHz, $CDCl_3$) δ 196.5, 143.2, 138.0, 134.9, 132.1, 130.3, 129.9, 128.9, 128.2, 21.6.

Phenyl(o-tolyl)methanone (3b).[25] Purification by column chromatography on a silica gel (ethyl acetate:petroleum ether = 1:50) afforded **3b** as a light yellow oil (28.6 mg, 73% yield); TLC (PE:EA, 10:1 v/v): R_f = 0.6; ^1H NMR (400 MHz, DMSO-d_6) δ 7.71−7.67 (m, 3H), 7.57−7.53 (m, 2H), 7.48−7.44 (m, 1H), 7.38−7.29 (m, 3H), 2.43 (s, 3H); $^{13}C\{^1H\}$ NMR (100 MHz, DMSO-d_6) δ 198.2, 138.7, 137.5, 136.2, 134.0, 131.4, 130.8, 130.1, 129.3, 128.5, 125.9, 19.9.

Phenyl(m-tolyl)methanone (3c).[26] Purification by column chromatography on a silica gel (ethyl acetate:petroleum ether = 1:50) afforded **3c** as a white solid (33.7 mg, 86% yield), mp 79−80 °C (lit.[26] 81−82 °C); TLC (PE:EA, 10:1 v/v): R_f = 0.65; ^1H NMR (400 MHz, $CDCl_3$) δ 7.81−7.79 (m, 2H), 7.63 (s, 1H), 7.61−7.57 (m, 2H), 7.50−7.46 (m, 2H), 7.41−7.34 (m, 2H), 2.42 (s, 3H); $^{13}C\{^1H\}$ NMR (100 MHz, $CDCl_3$) δ 196.9, 138.1, 137.8, 137.6, 133.1, 132.3, 130.4, 130.0, 128.2, 128.1, 127.3, 21.3.

(4-Methoxyphenyl)(phenyl)methanone (3d).[23] Purification by column chromatography on a silica gel (ethyl acetate:petroleum ether = 1:50) afforded **3d** as a white solid (36 mg, 85% yield), mp 85−86 °C (lit.[27] 85.9−86.5 °C); TLC (PE:EA, 10:1 v/v): R_f = 0.6; ^1H NMR (400 MHz, $CDCl_3$) δ 7.85−7.81 (m, 2H), 7.77−7.74 (m, 2H), 7.59−7.54 (m, 1H), 7.49−7.45 (m, 2H), 6.98−6.96 (m, 2H), 3.89 (s, 3H); $^{13}C\{^1H\}$ NMR (100 MHz, $CDCl_3$) δ 195.5, 163.2, 138.3, 132.5, 131.9, 130.2, 129.7, 128.2, 113.6, 55.5.

(2-Methoxyphenyl)(phenyl)methanone (3e).[25] Purification by column chromatography on a silica gel (ethyl acetate:petroleum ether = 1:50) afforded **3e** as a colorless oil (27.6 mg, 65% yield); TLC (PE:EA, 10:1 v/v): R_f = 0.65; ^1H NMR (400 MHz, $CDCl_3$) δ 7.83−7.80 (m, 2H), 7.57−7.53 (m, 1H), 7.49−7.41 (m, 3H), 7.38−7.35 (m, 1H), 7.06−7.02 (m, 1H), 6.99 (d, *J* = 8.4 Hz, 1H), 3.73 (s, 3H); $^{13}C\{^1H\}$ NMR (100 MHz, $CDCl_3$) δ 196.4, 157.3, 137.8, 132.9, 131.8, 129.8, 129.5, 128.8, 128.2, 120.5, 111.4, 55.6.

(3-Methoxyphenyl)(phenyl)methanone (3f).[25] Purification by column chromatography on a silica gel (ethyl acetate:petroleum

https://dx.doi.org/10.1021/acs.joc.0c02945
J. Org. Chem. 2021, 86, 5016−5025

ether = 1:50) afforded **3f** as a colorless oil (33.9 mg, 80% yield); TLC (PE:EA, 10:1 v/v): R_f = 0.65; ^{1}H NMR (400 MHz, $CDCl_3$) δ 7.82−7.80 (m, 2H), 7.61−7.57 (m, 1H), 7.50−7.46 (m, 2H), 7.40−7.32 (m, 3H), 7.15−7.12 (m, 1H), 3.86 (s, 3H); $^{13}C\{^1H\}$ NMR (100 MHz, $CDCl_3$) δ 196.5, 159.6, 138.9, 137.6, 132.4, 130.0, 129.2, 128.2122.8, 118.8, 114.3, 55.4.

*Benzophenone (**3g**).*[25] Purification by column chromatography on a silica gel (ethyl acetate:petroleum ether = 1:50) afforded **3g** as a white solid (31.7 mg, 87% yield), mp 47−48 °C (lit.[24] 48−49 °C); TLC (PE:EA, 10:1 v/v): R_f = 0.55; ^{1}H NMR (400 MHz, $CDCl_3$) δ 7.82−7.80 (m, 4H), 7.62−7.57 (m, 2H), 7.51−7.47 (m, 4H); $^{13}C\{^1H\}$ NMR (100 MHz, $CDCl_3$) δ 196.7, 137.6, 132.4, 130.0, 128.3.

*(1,1′-Biphenyl)-4-yl(phenyl)methanone (**3h**).*[27] Purification by column chromatography on a silica gel (ethyl acetate:petroleum ether = 1:50) afforded **3h** as a yellow solid (43.9 mg, 85% yield), mp 101−102 °C (lit.[27] 100.7−101.5 °C); TLC (PE:EA, 10:1 v/v): R_f = 0.55; ^{1}H NMR (400 MHz, $CDCl_3$) δ 7.90 (d, J = 7.7 Hz, 2H), 7.85 (d, J = 8.0 Hz, 2H), 7.71 (d, J = 7.7 Hz, 2H), 7.66 (d, J = 8.0 Hz, 2H), 7.61−7.59 (m, 1H), 7.53−7.47 (m, 4H), 7.43−7.41 (m, 1H); $^{13}C\{^1H\}$ NMR (100 MHz, $CDCl_3$) δ 196.3, 145.2, 140.0, 137.7, 136.2, 132.3, 130.7, 130.0, 128.9, 128.3, 128.2, 127.3, 126.9.

*1-(4-Benzoylphenyl)ethanone (**3i**).*[28] Purification by column chromatography on a silica gel (ethyl acetate:petroleum ether = 1:50) afforded **3i** as a white solid (33.1 mg, 74% yield), mp 81−83 °C (lit.[28] 83−84 °C); TLC (PE:EA, 10:1 v/v): R_f = 0.2; ^{1}H NMR (400 MHz, $CDCl_3$) δ 8.07−8.05 (m, 2H), 7.88−7.86 (m, 2H), 7.82−7.80 (m, 2H), 7.65−7.61 (m, 1H), 7.53−7.49 (m, 2H), 2.67 (s, 3H); $^{13}C\{^1H\}$ NMR (100 MHz, $CDCl_3$) δ 197.5, 196.0, 141.3, 139.6, 136.9, 133.0, 130.1, 130.0, 128.5, 128.1, 26.9.

*4-Benzoylbenzaldehyde (**3j**).*[28] Purification by column chromatography on a silica gel (ethyl acetate:petroleum ether = 1:50) afforded **3j** as a white solid (33.6 mg, 80% yield), mp 62−64 °C (lit.[28] 62−65 °C); TLC (PE:EA, 10:1 v/v): R_f = 0.65; ^{1}H NMR (400 MHz, $CDCl_3$) δ 10.13 (s, 1H), 8.0 (d, J = 8.3 Hz, 2H), 7.92 (d, J = 8.0 Hz, 2H), 7.82−7.79 (m, 2H), 7.65−7.61 (m, 1H), 7.53−7.49 (m, 2H); $^{13}C\{^1H\}$ NMR (100 MHz, $CDCl_3$) δ 195.8, 191.6, 142.5, 138.4, 136.7, 133.1, 130.3, 130.1, 129.5, 128.5.

*Ethyl 4-Benzoylbenzoate (**3k**).*[23] Purification by column chromatography on a silica gel (ethyl acetate:petroleum ether = 1:50) afforded **3k** as a yellow oil (46.3 mg, 90% yield); TLC (PE:EA, 10:1 v/v): R_f = 0.65; ^{1}H NMR (400 MHz, $CDCl_3$) δ 8.12 (d, J = 8.3 Hz, 2H), 7.85−7.79 (m, 4H), 7.64−7.60 (m, 1H), 7.52−7.48 (m, 2H), 4.43 (q, J = 7.2 Hz, 2H), 1.43 (t, J = 7.2 Hz, 3H); $^{13}C\{^1H\}$ NMR (100 MHz, $CDCl_3$) δ 196.0, 165.8, 141.2, 137.0, 133.6, 132.9, 130.1, 129.7, 129.4, 128.4, 61.4, 14.3.

*4-Cyanobenzophenone (**3l**).*[25] Purification by column chromatography on a silica gel (ethyl acetate:petroleum ether = 1:50) afforded **3l** as a white solid (35.5 mg, 85% yield), mp 111−112 °C (lit.[27] 110.8−111.1 °C); TLC (PE:EA, 10:1 v/v): R_f = 0.5; ^{1}H NMR (400 MHz, $CDCl_3$) δ 7.88 (d, J = 8.0 Hz, 2H), 7.81−7.72 (m, 4H), 7.66−7.63 (m, 1H), 7.54−7.50 (m, 2H); $^{13}C\{^1H\}$ NMR (100 MHz, $CDCl_3$) δ 195.0, 141.2, 136.3, 133.3, 132.2, 130.2, 130.1, 128.6, 118.0, 115.7.

*Phenyl(4-(trifluoromethyl)phenyl)methanone (**3m**).*[23] Purification by column chromatography on a silica gel (ethyl acetate:petroleum ether = 1:50) afforded **3m** as a white solid (44.5 mg, 88% yield), mp 111−112 °C (lit.[28] 110−112 °C); TLC (PE:EA, 10:1 v/v): R_f = 0.65; ^{1}H NMR (400 MHz, $CDCl_3$) δ 7.90 (d, J = 8.0 Hz, 2H), 7.82−7.80 (m, 2H), 7.76 (d, J = 8.0 Hz, 2H), 7.66−7.61 (m, 1H), 7.54−7.49 (m, 2H); $^{13}C\{^1H\}$ NMR (100 MHz, $CDCl_3$) δ 195.7, 140.9, 136.9, 133.9 (q, $^2J_{C\text{-}F}$ = 36.6 Hz), 133.2, 130.3, 130.2, 128.7, 125.5 (q, $^3J_{C\text{-}F}$ = 3.8 Hz), 123.8 (q, $^1J_{C\text{-}F}$ = 270.9 Hz); ^{19}F NMR δ −63.00 (s, 3F).

*Phenyl(3-(trifluoromethyl)phenyl)methanone (**3n**).*[25] Purification by column chromatography on a silica gel (ethyl acetate:petroleum ether = 1:50) afforded **3n** as a white solid (42.8 mg, 85% yield), mp 52−53 °C (lit.[29] 51−52 °C); TLC (PE:EA, 10:1 v/v): R_f = 0.65; ^{1}H NMR (400 MHz, $CDCl_3$) δ 8.07 (s, 1H), 7.98 (d, J = 7.8 Hz, 1H), 7.85 (d, J = 7.8 Hz, 1H), 7.81−7.78 (m, 2H), 7.66−7.61 (m, 2H), 7.54−7.50 (m, 2H); $^{13}C\{^1H\}$ NMR (100 MHz, $CDCl_3$) δ 195.2, 138.2, 136.7, 133.1, 133.0, 131.0 (q, $^2J_{C\text{-}F}$ = 32.8 Hz), 130.0, 128.9, 128.8 (q, $^3J_{C\text{-}F}$ = 3.7 Hz), 128.5, 126.7 (q, $^3J_{C\text{-}F}$ = 3.7 Hz), 123.7 (q, $^1J_{C\text{-}F}$ = 270.8 Hz); ^{19}F NMR δ −62.74 (s, 3F).

*(4-Fluorophenyl)(phenyl)methanone (**3o**).*[25] Purification by column chromatography on a silica gel (ethyl acetate:petroleum ether = 1:50) afforded **3o** as a white solid (30.1 mg 75% yield), mp 45−47 °C (lit.[28] 46−48 °C); TLC (PE:EA, 10:1 v/v): R_f = 0.65; ^{1}H NMR (400 MHz, $CDCl_3$) δ 7.87−7.83 (m, 2H), 7.78−7.76 (m, 2H), 7.62−7.58 (m, 1H), 7.51−7.47 (m, 2H), 7.19−7.14 (m, 2H); $^{13}C\{^1H\}$ NMR (100 MHz, $CDCl_3$) δ 195.2, 165.4 (d, ^1J = 252.5 Hz), 137.5, 133.8 (d, $^4J_{C\text{-}F}$ = 3.0 Hz), 132.6 (d, $^3J_{C\text{-}F}$ = 9.1 Hz), 132.4, 129.9, 128.3, 115.4 (d, $^2J_{C\text{-}F}$ = 21.7 Hz); ^{19}F NMR δ −105.9 (s, 1F).

*(4-Chlorophenyl)(phenyl)methanone (**3p**).*[25] Purification by column chromatography on a silica gel (ethyl acetate:petroleum ether = 1:50) afforded **3p** as a white solid (32.8 mg, 76% yield), mp 75−77 °C (lit.[28] 73−74 °C); TLC (PE:EA, 10:1 v/v): R_f = 0.65; ^{1}H NMR (400 MHz, $CDCl_3$) δ 7.79−7.74 (m, 4H), 7.62−7.58 (m, 1H), 7.51−7.45 (m, 4H); $^{13}C\{^1H\}$ NMR (100 MHz, $CDCl_3$) δ 195.5, 138.9, 137.2, 135.8, 132.6, 131.4, 129.9, 128.6, 128.4.

*(4-Bromophenyl)(phenyl)methanone (**3q**).*[25] Purification by column chromatography on a silica gel (ethyl acetate:petroleum ether = 1:50) afforded **3q** as a white solid (38.6 mg, 74% yield), mp 78−80 °C (lit.[30] 79−80 °C); TLC (PE:EA, 10:1 v/v): R_f = 0.65; ^{1}H NMR (400 MHz, $CDCl_3$) δ 7.78−7.74 (m, 2H), 7.62−7.58 (m, 5H), 7.51−7.45 (m, 2H); $^{13}C\{^1H\}$ NMR (100 MHz, $CDCl_3$) δ 195.6, 137.2, 136.3, 132.7, 131.6, 131.5, 129.9, 128.4, 127.5.

*(Naphthalen-6-yl)(phenyl)methanone (**3r**).*[28] Purification by column chromatography on a silica gel (ethyl acetate:petroleum ether = 1:50) afforded **3r** as a white solid (32.5 mg, 70% yield), mp 80−82 °C (lit.[28] 81−83 °C); TLC (PE:EA, 10:1 v/v): R_f = 0.5; ^{1}H NMR (400 MHz, $CDCl_3$) δ 8.27 (s, 1H), 7.95−7.86 (m, 6H), 7.65−7.50 (m, 5H); $^{13}C\{^1H\}$ NMR (100 MHz, $CDCl_3$) δ 196.7, 137.9, 135.3, 134.8, 132.4, 132.2, 131.8, 130.1, 129.4, 128.34, 128.31, 128.29, 127.8, 126.8, 125.8.

*(6-Fluoropyridin-3-yl)(phenyl)methanone (**3s**).*[16] Purification by column chromatography on a silica gel (ethyl acetate:petroleum ether = 1:50) afforded **3s** as a white solid (17.4 mg, 43% yield), mp 42−44 °C; TLC (PE:EA, 10:1 v/v): R_f = 0.25; ^{1}H NMR (400 MHz, $CDCl_3$) δ 8.66 (d, J = 2.3 Hz, 1H), 8.32−8.27 (m, 1H), 7.81−7.79 (m, 2H), 7.67−7.63 (m, 1H), 7.55−7.51 (m, 2H), 7.09 (dd, J_1 = 8.7, 2.7 Hz, 1H); $^{13}C\{^1H\}$ NMR (100 MHz, $CDCl_3$) δ 193.2, 165.2 (d, $^1J_{C\text{-}F}$ = 244.3 Hz), 150.3 (d, $^3J_{C\text{-}F}$ = 16.1 Hz), 142.8 (d, $^3J_{C\text{-}F}$ = 9.1 Hz), 136.6, 133.2, 131.4 (d, $^4J_{C\text{-}F}$ = 4.5 Hz), 129.8, 128.6, 109.7 (d, $^2J_{C\text{-}F}$ = 37.1 Hz); ^{19}F NMR δ −61.45 (s, 1F).

*4-Methoxy-4′-methylbenzophenone (**3b′**).*[31] Purification by column chromatography on a silica gel (ethyl acetate:petroleum ether = 1:50) afforded **3b′** as a white solid (44.3 mg, 83% yield), mp 89−90 °C (lit.[31] 90−91 °C); TLC (PE:EA, 10:1 v/v): R_f = 0.5; ^{1}H NMR (400 MHz, DMSO-d_6) δ 7.73 (d, J = 8.6 Hz, 2H), 7.60 (d, J = 7.8 Hz, 2H), 7.35 (d, J = 7.7 Hz, 2H), 7.08 (d, J = 8.6 Hz, 2H), 3.85 (s, 3H), 2.40 (s, 3H); $^{13}C\{^1H\}$ NMR (100 MHz, DMSO-d_6) δ 194.1, 162.7, 142.4, 135.0, 132.0, 129.6, 129.5, 129.0, 113.8, 55.5, 21.1.

*Mesityl(p-tolyl)methanone (**3c′**).*[16] Purification by column chromatography on a silica gel (ethyl acetate:petroleum ether = 1:50) afforded **3c′** as a white solid (34.8 mg, 73% yield), mp 39−40 °C (lit.[32] 39−40 °C); TLC (PE:EA, 10:1 v/v): R_f = 0.5; ^{1}H NMR (400 MHz, $CDCl_3$) δ 7.70 (d, J = 8.0 Hz, 2H), 7.24 (d, J = 8.0 Hz, 2H), 6.89 (s, 2H), 2.41 (s, 3H), 2.33 (s, 3H), 2.08 (s, 6H); $^{13}C\{^1H\}$ NMR (100 MHz, $CDCl_3$) δ 200.4, 144.5, 138.3, 137.0, 134.8, 134.1, 129.53, 129.46, 128.2, 21.7, 21.1, 19.3.

*4-Trifluoromethyl-4′-methylbenzophenone (**3d′**).*[31] Purification by column chromatography on a silica gel (ethyl acetate:petroleum ether = 1:50) afforded **3d′** as a white solid (5.8 mg, 10% yield), mp 133−135 °C (lit.[31] 134−135 °C); TLC (PE:EA, 10:1 v/v): R_f = 0.5; ^{1}H NMR (400 MHz, $CDCl_3$) δ 7.87 (d, J = 8.0 Hz, 2H), 7.75−7.71 (m, 4H), 7.30 (d, J = 8.0 Hz, 2H), 2.45 (s, 3H). $^{13}C\{^1H\}$ NMR (100 MHz, $CDCl_3$) δ 195.2, 144.1, 141.1, 134.1, 133.5 (q, $^1J_{C\text{-}F}$ = 32.5 Hz), 130.3, 130.0, 129.2, 125.2 (q, $^2J_{C\text{-}F}$ = 3.7 Hz), 123.7 (q, $^1J_{C\text{-}F}$ = 270.9 Hz), 21.7; ^{19}F NMR δ −63.00 (s, 3F).

https://dx.doi.org/10.1021/acs.joc.0c02945
J. Org. Chem. 2021, 86, 5016−5025

*4-Fluoro-4′-methylbenzophenone (**3e′**).*[30] Purification by column chromatography on a silica gel (ethyl acetate:petroleum ether = 1:50) afforded **3e′** as a white solid (30 mg, 70% yield), mp 93−95 °C (lit.[30] 97−98 °C); TLC (PE:EA, 10:1 v/v): R_f = 0.5; ^{1}H NMR (400 MHz, $CDCl_3$) δ 7.84−7.81 (m, 2H), 7.69 (d, J = 8.0 Hz, 2H), 7.29 (d, J = 7.9 Hz, 2H), 7.17−7.13 (m, 2H), 2.45 (s, 3H). $^{13}C\{^1H\}$ NMR (100 MHz, $CDCl_3$) δ 195.0, 165.2 (d, $^1J_{C-F}$ = 252.0 Hz), 143.3, 134.8, 134.1 (d, $^4J_{C-F}$ = 3.0 Hz), 132.5, (d, $^3J_{C-F}$ = 9.0 Hz, 130.1, 129.0, 115.3 (d, $^2J_{C-F}$ = 21.6 Hz), 21.7.

*4-Chloro-4′-methylbenzophenone (**3f′**).*[16] Purification by column chromatography on a silica gel (ethyl acetate:petroleum ether = 1:50) afforded **3f′** as a white solid (31 mg, 67% yield), mp 128−129 °C (lit.[29] 128−129 °C); TLC (PE:EA, 10:1 v/v): R_f = 0.4; ^{1}H NMR (400 MHz, $CDCl_3$) δ 7.75−7.72 (m, 2H), 7.71−7.67 (m, 2H), 7.47−7.44 (m, 2H), 7.30−7.28 (m, 2H), 2.45 (s, 3H). $^{13}C\{^1H\}$ NMR (100 MHz, $CDCl_3$) δ 195.2, 143.5, 138.6, 136.2, 134.5, 131.3, 130.1, 129.1, 128.5, 21.7.

*(Naphthalen-3-yl)(p-tolyl)methanone (**3g′**).*[33] Purification by column chromatography on a silica gel (ethyl acetate:petroleum ether = 1:50) afforded **3g′** as a white solid (35.1 mg, 70% yield), mp 85−87 °C (lit.[30] 85−87 °C); TLC (PE:EA, 10:1 v/v): R_f = 0.5; ^{1}H NMR (400 MHz, $CDCl_3$) δ 8.25 (s, 1H), 7.94−7.90 (m, 4H), 7.79 (d, J = 8.0 Hz, 2H), 7.63−7.54 (m, 2H), 7.32 (d, J = 8.0 Hz, 2H), 2.47 (s, 3H); $^{13}C\{^1H\}$ NMR (100 MHz, $CDCl_3$) δ 196.5, 143.2, 135.1, 132.2, 131.6, 130.3, 129.0, 128.2, 128.2, 127.8, 126.7, 125.8, 91.4, 21.7.

*3-Phenyl-1-(p-tolyl)propan-1-one (**3h′**).*[31] Purification by column chromatography on a silica gel (ethyl acetate:petroleum ether = 1:50) afforded **3h′** as a yellow oil (39.8 mg, 88% yield), mp 61−63 °C (lit.[31] 65−66 °C); TLC (PE:EA, 10:1 v/v): R_f = 0.5; ^{1}H NMR (400 MHz, $CDCl_3$) δ 7.86 (d, J = 8.0 Hz, 2H), 7.32−7.18 (m, 7H), 3.28 (t, J = 7.8 Hz, 2H), 3.06 (t, J = 7.8 Hz, 2H), 2.40 (s, 3H). $^{13}C\{^1H\}$ NMR (100 MHz, $CDCl_3$) δ 198.9, 143.8, 141.4, 134.3, 129.2, 128.5, 128.4, 128.1, 126.1, 40.4, 30.2, 21.6.

*Cyclohexyl(p-tolyl)methanone (**3i′**).*[31] Purification by column chromatography on a silica gel (ethyl acetate:petroleum ether = 1:50) afforded **3i′** as a colorless oil (35.4 mg, 87% yield), mp 60−62 °C (lit.[31] 62−63 °C); TLC (PE:EA, 10:1 v/v): R_f = 0.5; ^{1}H NMR (400 MHz, $CDCl_3$) δ 7.86 (d, J = 8.0 Hz, 2H), 7.27 (d, J = 8.0 Hz, 2H), 3.29−3.22 (m, 1H), 2.43 (s, 3H), 1.91−1.84 (m, 4H), 1.73 (d, J = 12.8 Hz, 1H), 1.54−1.22 (m, 5H). $^{13}C\{^1H\}$ NMR (100 MHz, $CDCl_3$) δ 203.5, 143.4, 133.7, 129.2, 128.3, 45.5, 29.4, 25.94, 25.85, 21.6.

*3-Methyl-1-(p-tolyl)butan-1-one (**3j′**).*[16] Purification by column chromatography on a silica gel (ethyl acetate:petroleum ether = 1:50) afforded **3j′** as a colorless oil (30.6 mg, 86% yield); TLC (PE:EA, 10:1 v/v): R_f = 0.5; ^{1}H NMR (400 MHz, $CDCl_3$) δ 7.86 (d, J = 8.0 Hz, 2H), 7.25 (d, J = 8.0 Hz, 2H), 2.81 (d, J = 7.2 Hz, 2H), 2.41 (s, 3H), 2.32−2.25 (m, 1H), 0.99 (d, J = 6.8 Hz, 6H). $^{13}C\{^1H\}$ NMR (100 MHz, $CDCl_3$) δ 200.0, 143.6, 134.9, 129.2, 128.2, 47.4, 25.3, 22.8, 21.6.

*2,2,6,6-Tetramethylpiperidin-1-yl Benzoate (**3a″**).*[16] Purification by column chromatography on a silica gel (ethyl acetate:petroleum ether = 1:50) afforded **3a″** as a white solid (42.3 mg, 80% yield), mp 84−86 °C (lit.[34] 85−87 °C); TLC (PE:EA, 10:1 v/v): R_f = 0.5; ^{1}H NMR (400 MHz, $CDCl_3$) δ 8.10−8.07 (m, 2H), 7.59−7.56 (m, 2H), 7.48−7.44 (m, 2H), 1.83−1.69 (m, 3H), 1.64−1.57 (m, 2H), 1.48−1.43 (m, 1H), 1.28 (s, 6H), 1.12 (s, 6H). $^{13}C\{^1H\}$ NMR (100 MHz, $CDCl_3$) δ 166.4, 132.8, 129.7, 129.6, 128.4, 60.4, 39.1, 32.0, 20.8, 17.0.

*N-(p-Tolyl)benzamide (**5**).*[20] Purification by column chromatography on a silica gel (ethyl acetate:petroleum ether = 1:10) afforded **5** as a white solid (31 mg, 73% yield). mp 156−158 °C (lit.[16] 158−159 °C); TLC (PE:EA, 2:1 v/v): R_f = 0.75; ^{1}H NMR (400 MHz, $CDCl_3$) δ 7.91 (s, 1H), 7.85 (d, J = 7.6 Hz, 2H), 7.53−7.43 (m, 5H), 7.16 (d, J = 8.0 Hz, 2H), 2.33 (s, 3H). $^{13}C\{^1H\}$ NMR (100 MHz, $CDCl_3$) δ 165.7, 135.4, 135.1, 134.2, 131.7, 129.6, 128.7, 127.0, 120.4, 20.9.

*1-(tert-Butyl) 2-(4-(Methoxycarbonyl)phenyl)pyrrolidine-1,2-dicarboxylate (**8**).*[20] Purification by column chromatography on a silica gel (ethyl acetate:petroleum ether = 1:5) afforded **3a″** as a yellowish oil (62.5 mg, 89% yield). TLC (PE:EA, 2:1 v/v): R_f = 0.4; ^{1}H NMR (400 MHz, $CDCl_3$) δ 8.08−8.04 (m, 2H), 7.20−7.16 (m, 2H), 4.52 (dd, J = 8.6, 4.2 Hz, 0.4H), 4.45 (dd, J = 8.6, 4.2 Hz, 0.6H), 3.91−3.90 (m, 3H), 3.65−3.42 (m, 2H), 2.44−2.29 (m, 1H), 2.21−2.11 (m, 1H), 2.09−1.91 (m, 2H), 1.47−1.45 (m, 9H). $^{13}C\{^1H\}$ NMR (100 MHz, $CDCl_3$) δ 171.1, 171.0, 166.3, 166.2, 154.5, 154.2, 153.7, 131.2, 131.1, 127.8, 127.7, 121.5, 121.1, 80.4, 80.2, 59.2, 59.1, 52.2, 52.1, 46.6, 46.4, 31.0, 30.0, 28.4, 24.5, 23.7.

■ ASSOCIATED CONTENT

Supporting Information

The Supporting Information is available free of charge at https://pubs.acs.org/doi/10.1021/acs.joc.0c02945.

Optimization studies of decarboxylative C−C cross-coupling; UV−vis absorption spectra of all photocatalysts; fluorescence emission spectra of **DCPP**; cyclic voltammograms of **DCPP**; transient absorption spectra and luminescence decays of **DCPP**; devices for the photocatalytic reactions; and ^{1}H and ^{13}C NMR spectra for all compounds (PDF)

■ AUTHOR INFORMATION

Corresponding Authors

Xiaoqiang Yu − *State Key Laboratory of Fine Chemicals, Dalian University of Technology, Dalian 116023, Liaoning, China;* orcid.org/0000-0001-9396-3882; Email: yuxiaoqiang@dlut.edu.cn

Ming Bao − *State Key Laboratory of Fine Chemicals, Dalian University of Technology, Dalian 116023, Liaoning, China;* orcid.org/0000-0002-5179-3499; Email: mingbao@dlut.edu.cn

Authors

Min He − *State Key Laboratory of Fine Chemicals, Dalian University of Technology, Dalian 116023, Liaoning, China*

Yi Wang − *State Key Laboratory of Fine Chemicals, Dalian University of Technology, Dalian 116023, Liaoning, China*

Fei Li − *State Key Laboratory of Fine Chemicals, Dalian University of Technology, Dalian 116023, Liaoning, China;* orcid.org/0000-0002-3686-7576

Complete contact information is available at: https://pubs.acs.org/10.1021/acs.joc.0c02945

Notes

The authors declare no competing financial interest.

■ ACKNOWLEDGMENTS

We are grateful to the National Natural Science Foundation of China (nos. 21872015 and 21572028) for their financial support. This work was also supported by the LiaoNing Natural Science Foundation of China (201602181), LiaoNing Revitalization Talents Program (XLYC1802030), and Outstanding Young Scholars Development Growth Plan of universities in LiaoNing Province (LJQ2015027). We thank Prof. Paul Freimuth from the Brookhaven National Laboratory for editing the manuscript.

■ REFERENCES

(1) (a) Nicewicz, D. A.; MacMillan, D. W. C. Merging Photoredox Catalysis with Organocatalysis: The Direct Asymmetric Alkylation of Aldehydes. *Science* **2008**, *322*, 77−80. (b) Yoon, T. P.; Ischay, M. A.; Du, J. Visible Light Photocatalysis as a Greener Approach to Photochemical Synthesis. *Nat. Chem.* **2010**, *2*, 527−532. (c) Nar-

ayanam, J. M. R.; Stephenson, C. R. J. Visible Light Photoredox Catalysis: Applications in Organic Synthesis. *Chem. Soc. Rev.* **2011**, *40*, 102−113. (d) Xuan, J.; Xiao, W. J. Visible-Light Photoredox Catalysis. *Angew. Chem., Int. Ed.* **2012**, *51*, 6828−6838. (e) Prier, C. K.; Rankic, D. A.; MacMillan, D. W. C. Visible Light Photoredox Catalysis with Transition Metal Complexes: Applications in Organic Synthesis. *Chem. Rev.* **2013**, *113*, 5322−5363. (f) Marzo, L.; Pagire, S. K.; Reiser, O.; König, B. Visible-Light Photocatalysis: Does it Make a Difference in Organic Synthesis? *Angew. Chem., Int. Ed.* **2018**, *57*, 10034−10072. (h) Romero, N. A.; Nicewicz, D. A. Organic Photoredox Catalysis. *Chem. Rev.* **2016**, *116*, 10075−10166.

(2) (a) Chen, T. Q.; MacMillan, D. W. C. A Metallaphotoredox Strategy for the Cross-Electrophile Coupling of Alpha-Chloro Carbonyls with Aryl Halides. *Angew. Chem., Int. Ed.* **2019**, *58*, 14584−14588. (b) Lu, F. D.; Liu, D.; Zhu, L.; Lu, L. Q.; Yang, Q.; Zhou, Q. Q.; Wei, Y.; Lan, Y.; Xiao, W. J. Asymmetric Propargylic Radical Cyanation Enabled by Dual Organophotoredox and Copper Catalysis. *J. Am. Chem. Soc.* **2019**, *141*, 6167−6172.

(3) (a) Lu, Z.; Yoon, T. P. Visible Light Photocatalysis of [2+2] Styrene Cycloadditions by Energy Transfer. *Angew. Chem., Int. Ed.* **2012**, *51*, 10329−10332. (b) Ding, W.; Ho, C. C.; Yoshikai, N. Photosensitized, Energy-Transfer-Mediated Cyclization of 2-(1-Arylvinyl)benzaldehydes to Anthracen-9-(10*H*)-ones. *Org. Lett.* **2019**, *21*, 1202−1206. (c) Dewanji, A.; Krach, P. E.; Rueping, M. The Dual role of Benzophenone in Visible-Light/Nickel Photoredox-Catalyzed C-H Arylations: Hydrogen-Atom Transfer and Energy Transfer. *Angew. Chem., Int. Ed.* **2019**, *58*, 3566−3570. (d) Zhou, Q. Q.; Zou, Y. Q.; Lu, L. Q.; Xiao, W. J. Visible-Light-Induced Organic Photochemical Reactions through Energy-Transfer Pathways. *Angew. Chem., Int. Ed.* **2019**, *58*, 1586−1604.

(4) (a) Koike, T.; Akita, M. Visible-Light Radical Reaction Designed by Ru- and Ir-Based Photoredox Catalysis. *Inorg. Chem. Front.* **2014**, *1*, 562−576. (b) Xie, J.; Jin, H.; Hashmi, A. S. K. The Recent Achievements of Redox-Neutral Radical C-C Cross-Coupling Enabled by Visible-Light. *Chem. Soc. Rev.* **2017**, *46*, 5193−5203. (c) Twilton, J.; Le, C.; Zhang, P.; Shaw, M. H.; Evans, R. W.; MacMillan, D. W. C. The Merger of Transition Metal and Photocatalysis. *Nat. Rev. Chem.* **2017**, *1*, 1−18.

(5) Nicewicz, D. A.; Nguyen, T. M. Recent Applications of Organic Dyes as Photoredox Catalysts in Organic Synthesis. *ACS Catal.* **2013**, *4*, 355−360.

(6) (a) Majek, M.; Wangelin, A. J. Mechanistic Perspectives on Organic Photoredox Catalysis for Aromatic Substitutions. *Acc. Chem. Res.* **2016**, *49*, 2316−2327. (b) Srivastava, V.; Singh, P. P. Eosin Y Catalysed Photoredox Synthesis: a Review. *RSC Adv.* **2017**, *7*, 31377−31392.

(7) (a) Joshi-Pangu, A.; Lévesque, F.; Roth, H. G.; Oliver, S. F.; Campeau, L.-C.; Nicewicz, D.; DiRocco, D. A. Acridinium-Based Photocatalysts: A Sustainable Option in Photoredox Catalysis. *J. Org. Chem.* **2016**, *81*, 7244−7249. (b) Fischer, C.; Kerzig, C.; Zilate, B.; Wenger, O. S.; Sparr, C. Modulation of Acridinium Organophotoredox Catalysts Guided by Photophysical Studies. *ACS Catal.* **2019**, *10*, 210−215. (c) Fischer, C.; Sparr, C. Direct Transformation of Esters into Heterocyclic Fluorophores. *Angew. Chem., Int. Ed.* **2018**, *57*, 2436−2440.

(8) (a) Luo, J.; Zhang, J. Donor−Acceptor Fluorophores for Visible-Light-Promoted Organic Synthesis: Photoredox/Ni Dual Catalytic $C(sp^3)$−$C(sp^2)$ Cross-Coupling. *ACS Catal.* **2016**, *6*, 873−877. (b) Huang, H.; Yu, C.; Zhang, Y.; Zhang, Y.; Mariano, P. S.; Wang, W. Chemo- and Regioselective Organo-Photoredox Catalyzed Hydroformylation of Styrenes via a Radical Pathway. *J. Am. Chem. Soc.* **2017**, *139*, 9799−9802. (c) Meng, Q.-Y.; Schirmer, T. E.; Berger, A. L.; Donabauer, K.; König, B. Photocarboxylation of Benzylic C-H Bonds. *J. Am. Chem. Soc.* **2019**, *141*, 11393−11397. (d) Zhao, B.; Shang, R.; Cheng, W. M.; Fu, Y. Decarboxylative Formylation of Aryl Halides with Glyoxylic Acid by Merging Organophotoredox with Palladium Catalysis. *Org. Chem. Front.* **2018**, *5*, 1782−1786.

(9) (a) Jhun, B. H.; Yi, S. Y.; Jeong, D.; Cho, J.; Park, S. Y.; You, Y. Aggregation of an *n*-π^* Molecule Induces Fluorescence Turn-On. *J. Phys. Chem. C* **2017**, *121*, 11907−11914. (b) Sugiyama, R.; Nakatani, T.; Nishimura, S.; Takenaka, K.; Ozaki, T.; Asamizu, S.; Onaka, H.; Kakeya, H. Chemical Interactions of Cryptic Actinomycete Metabolite 5-Alkyl-1,2,3,4-Tetrahydroquinolines through Aggregate Formation. *Angew. Chem., Int. Ed.* **2019**, *58*, 13486−13491. (c) Zhao, Z.; Zhang, H.; Lam, J. W. Y.; Tang, B. Z. Aggregation-Induced Emission: New Vistas at the Aggregate Level. *Angew. Chem., Int. Ed.* **2020**, *59*, 9888−9907.

(10) (a) Hunter, C. A.; Sanders, J. K. M. The Nature of π-π Interactions. *J. Am. Chem. Soc.* **1990**, *112*, 5525−5534. (b) Chen, Z.; Lohr, A.; Saha-Möller, C. R.; Würthner, F. Self-Assembled π-Stacks of Functional Dyes in Solution: Structural and Thermodynamic Features. *Chem. Soc. Rev.* **2009**, *38*, 564−584. (c) Wheeler, S. E.; Bloom, J. W. G. Toward a More Complete Understanding of Noncovalent Interactions Involving Aromatic Rings. *J. Phys. Chem. A* **2014**, *118*, 6133−6147.

(11) (a) Tang, B. Z.; Geng, Y.; Lam, J. W. Y.; Li, B.; Jing, X.; Wang, X.; Wang, F.; Pakhomov, A. B.; Zhang, X. X. Processible Nanostructured Materials with Electrical Conductivity and Magnetic Susceptibility: Preparation and Properties of Maghemite/Polyaniline Nanocomposite Films. *Chem. Mater.* **1999**, *11*, 1581−1589. (b) Liu, X.; Cole, J. M.; Chow, P. C. Y.; Zhang, L.; Tan, Y.; Zhao, T. Dye Aggregation and Complex Formation Effects in 7-(Diethylamino)-Coumarin-3-Carboxylic Acid. *J. Phys. Chem. C* **2014**, *118*, 13042−13051. (c) Liu, Z.; Zhou, C.; Lei, T.; Nan, X. L.; Chen, B.; Tung, C. H.; Wu, L. Z. Aggregation-Enabled Intermolecular Photo[2+2]-cycloaddition of Aryl Terminal Olefins by Visible-Lightcatalysis. *CCS Chem.* **2020**, *2*, 582−588.

(12) (a) Crisenza, G. E. M.; Mazzarella, D.; Melchiorre, P. Synthetic Methods Driven by the Photoactivity of Electron Donor-Acceptor Complexes. *J. Am. Chem. Soc.* **2020**, *142*, 5461−5476. (b) Fu, M. C.; Wang, J. X.; Shang, R. Triphenylphosphine-Catalyzed Alkylative Iododecarboxylation with Lithium Iodide under Visible Light. *Org. Lett.* **2020**, *22*, 8572−8577. (c) Fu, M. C.; Shang, R.; Zhao, B.; Wang, B.; Fu, Y. Photocatalytic Decarboxylative Alkylations Mediated by Triphenylphosphine and Sodium Iodide. *Science* **2019**, *363*, 1429−1434.

(13) Hong, Y.; Lam, J. W. Y.; Tang, B. Z. Aggregation-Induced Emission: Phenomenon, Mechanism and Applications. *Chem. Commun.* **2009**, 4332−4353.

(14) Amer, A. M.; El-Farargy, A. F.; Yousif, N. M.; Fayed, A. A. Synthesis and Pharmacological Activities of some Dibenzopyrazolocinnolines and Dibenzopyridazinoquinoxalines. *Chem. Heterocycl. Compd.* **2011**, *47*, 101−107.

(15) Kumar, G. R.; Sarkar, S. K.; Thilagar, P. Aggregation-Induced Emission and Sensing Characteristics of Triarylborane−Oligothiophene−Dicyanovinyl Triads. *Chem. Eur. J.* **2016**, *22*, 17215−17225.

(16) Reckmeier, C. J.; Schneider, J.; Xiong, Y.; Häusler, J.; Kasák, P.; Schnick, W.; Rogach, A. L. Aggregated Molecular Fluorophores in the Ammonothermal Synthesis of Carbon Dots. *Chem. Mater.* **2017**, *29*, 10352−10361.

(17) (a) Cheng, W. M.; Shang, R.; Yu, H. Z.; Fu, Y. Room-Temperature Decarboxylative Couplings of Alpha-Oxo Carboxylates with Aryl Halides by Merging Photoredox with Palladium Catalysis. *Chem. Eur. J.* **2015**, *21*, 13191−13195. (b) Chu, L.; Lipshultz, J. M.; MacMillan, D. W. C. Merging Photoredox and Nickel Catalysis: The Direct Synthesis of Ketones by the Decarboxylative Arylation of α-Oxo Acids. *Angew. Chem., Int. Ed.* **2015**, *54*, 7929−7933.

(18) The transient absorption spectrum was examined with laser pulses of 7 ns duration irradiation at λ_{pump} = 355 nm in a DMF solvent. Figure S3 shows an excited-state absorption feature at λ = 420 nm.

(19) In cyclic voltammetry, reduction of **DCPP** in deuterated DMF with 0.1 M $TBAPF_6$ results in reversible waves from which there are potentials of −0.82 V vs saturated calomel electrode (SCE). The energy level of the lowest-lying excited state is determined by calculating the energy of the wavelength at which the substrate's UV−vis absorption and emission spectra overlap, $E_{0,0}$ = 2.92 eV. $E_{red}([\mathbf{DCPP}]_n^*/[\mathbf{DCPP}]_n^{\cdot-})$ = +2.10 V vs. SCE in DMF.

https://dx.doi.org/10.1021/acs.joc.0c02945
J. Org. Chem. 2021, 86, 5016−5025

(20) Liu, J.; Liu, Q.; Yi, H.; Qin, C.; Bai, R. B.; Qi, X. T.; Lan, Y.; Lei, A. W. Visible-Light-Mediated Decarboxylation/Oxidative Amidation of α-Keto Acids with Amines under Mild Reaction Conditions Using O_2. *Angew. Chem., Int. Ed.* **2014**, *53*, 502−506.
(21) Welin, E. R.; Le, C.; Arias-Rotondo, D. M.; McCusker, J. K.; MacMillan, D. W. C. Photosensitized, Energy Transfer-Mediated Organometallic Catalysis through Electronically Excited Nickel(II). *Science* **2017**, *355*, 380−385.
(22) Wadhwa, K.; Yang, C.; West, P. R.; Deming, K. C.; Chemburkar, S. R.; Reddy, R. E. Synthesis of Arylglyoxylic Acids and their Collision-Induced Dissociation. *Synth. Commun.* **2008**, *38*, 4434−4444.
(23) Gooßen, L. J.; Rudolphi, F.; Oppel, C.; Rodríguez, N. Synthesis of Ketones from α-Oxocarboxylates and Aryl Bromides by Cu/Pd-Catalyzed Decarboxylative Cross-Coupling. *Angew. Chem., Int. Ed.* **2008**, *47*, 3043−3045.
(24) Wang, H. Q.; Wang, Z.; Huang, H. C.; Tan, J. J.; Xu, K. KO^{t}Bu-Promoted Oxidation of (Hetero)benzylic C_{sp^3}−H to Ketones with Molecular Oxygen. *Org. Lett.* **2016**, *18*, 5680−5683.
(25) Li, M. Z.; Wang, C.; Ge, H. B. Pd(II)-Catalyzed Decarboxylative Cross-Coupling of Potassium Aryltrifluoroborates with α-Oxocarboxylic Acids at Room Temperature. *Org. Lett.* **2011**, *13*, 2062−2064.
(26) Wang, C.; Huang, L. Y.; Wang, F. Z.; Zou, G. Highly Efficient Synthesis of Aryl Ketones by PEPPSI-Palladium Catalyzed Acylative Suzuki Coupling of Amides with Diarylborinic Acids. *Tetrahedron Lett.* **2018**, *59*, 2299−2301.
(27) Zhao, H. Y.; Du, H. Y.; Yuan, X. R.; Wang, T. J.; Han, W. Iron-Catalyzed Carbonylation of Aryl Halides with Arylborons using Stoichiometric Chloroform as the Carbon Monoxide Source. *Green Chem.* **2016**, *18*, 5782−5787.
(28) Wang, G. Z.; Li, X. L.; Dai, J.J.; Xu, H. J. AIBN-Catalyzed Oxidative Cleavage of Gem-disubstituted Alkenes with O_2 as an Oxidant. *J. Org. Chem.* **2014**, *79*, 7220−7225.
(29) Hao, W. Y.; Liu, H. Y.; Yin, L.; Cai, M. Z. Phosphine-Free, Heterogeneous Palladium-Catalyzed Atom-Efficient Carbonylative Cross-Coupling of Triarylbismuths with Aryl Iodides: Synthesis of Biaryl Ketones. *J. Org. Chem.* **2016**, *81*, 4244−4251.
(30) Wang, X.; Huang, Y. B.; Xu, Y. L.; Tang, X. D.; Wu, W. Q.; Jiang, H. F. Palladium-Catalyzed Denitrogenative Synthesis of Aryl Ketones from Arylhydrazines and Nitriles using O_2 as Sole Oxidant. *J. Org. Chem.* **2017**, *82*, 2211−2218.
(31) Li, X. J.; Zou, G. Palladium-catalyzed Acylative Cross-Coupling of Amides with Diarylborinic Acids and Sodium Tetraarylborates. *J. Organomet. Chem.* **2015**, *794*, 136−145.
(32) Wiegers, K. E.; Smith, S. G. Kinetics and Mechanism of Lithium Aluminum Hydride and Lithium Alkoxyaluminohydride Reductions of Ketones in Diethyl Ether. *J. Am. Chem. Soc.* **1977**, *99*, 1480−1487.
(33) Si, S. F.; Wang, C.; Zhang, N.; Zou, G. Palladium-Catalyzed Room-Temperature Acylative Suzuki Coupling of High-Order Aryl Borons with Carboxylic Acids. *J. Org. Chem.* **2016**, *81*, 4364−4370.
(34) Hossian, A.; Manna, M. K.; Manna, K.; Jana, R. Palladium-Catalyzed Decarboxylative, Decarbonylative and Dehydrogenative C(sp^2)−H Acylation at Room Temperature. *Org. Biomol. Chem.* **2017**, *15*, 6592−6603.

https://dx.doi.org/10.1021/acs.joc.0c02945
J. Org. Chem. 2021, 86, 5016−5025